

Supplementary Materials

Perpendicular compensated ferrimagnetic tunnel junctions

Qi Liu^{1,2,#}, Pengfei Liu^{3,4,#}, Xiaowen Li¹, Shanquan Chen¹, Sixia Hu², Yao Wang², Zedong Xu⁴, Songbai Hu⁵, Mao Ye⁶, Kaiyou Wang^{3,7}, Lang Chen^{1,8,9}

¹Department of Physics, Southern University of Science and Technology, Shenzhen 518055, Guangdong, China.

²Core Research Facilities, Southern University of Science and Technology, Shenzhen 518055, Guangdong, China.

³State Key Laboratory of Semiconductor Physics and Chip Technologies, Institute of Semiconductors, Chinese Academy of Sciences, Beijing 100083, China.

⁴School of Electronics and Information Engineering, Tiangong University, Tianjin 300387, China.

⁵School of Physical Science, Great Bay University, Dongguan 523429, Guangdong, China.

⁶School of Physics and Materials Science, Guangzhou University, Guangzhou 510006, Guangdong, China.

⁷Center of Materials Science and Optoelectronics Engineering, University of Chinese Academy of Sciences, Beijing 100049, China.

⁸State Key Laboratory of Quantum Functional Materials, Southern University of Science and Technology, Shenzhen 518055, Guangdong, China.

⁹Guangdong Basic Research Center of Excellence for Quantum Science, Southern University of Science and Technology, Shenzhen 518055, Guangdong, China.

[#]These authors contributed equally to this work.

Correspondence to: Prof. Kaiyou Wang, State Key Laboratory of Semiconductor Physics and Chip Technologies, Institute of Semiconductors, Chinese Academy of Sciences, Beijing 100083, China; Center of Materials Science and Optoelectronics Engineering, University of Chinese Academy of Sciences, Beijing 100049, China. E-

mail: kywang@semi.ac.cn; Prof. Lang Chen, Department of Physics, Southern University of Science and Technology, Shenzhen 518055, Guangdong, China; State Key Laboratory of Quantum Functional Materials, Southern University of Science and Technology, Shenzhen 518055, Guangdong, China; Guangdong Basic Research Center of Excellence for Quantum Science, Southern University of Science and Technology, Shenzhen 518055, Guangdong, China. E-mail: chenlang@sustech.edu.cn

ORCID: Kaiyou Wang (0000-0002-6017-7575), Lang Chen (0000-0003-2460-8232)

Contents

SI 1. Flow chart for fabrication of tunnel junction devices.

SI 2. TEM of the heterostructures.

SI 3. The temperature-dependent anomalous Hall effect (AHE) and magnetic characteristic of CoGd.

SI 4. Temperature-dependent magnetization of NCO.

SI 5. Angular dependence of the TMR.

SI 6. Angle-dependent AHE loops.

SI 7. The size-dependent TMR of our ferrimagnetic tunnel junctions.

SI 8. The range of assisted magnetic field for thermal modulation.

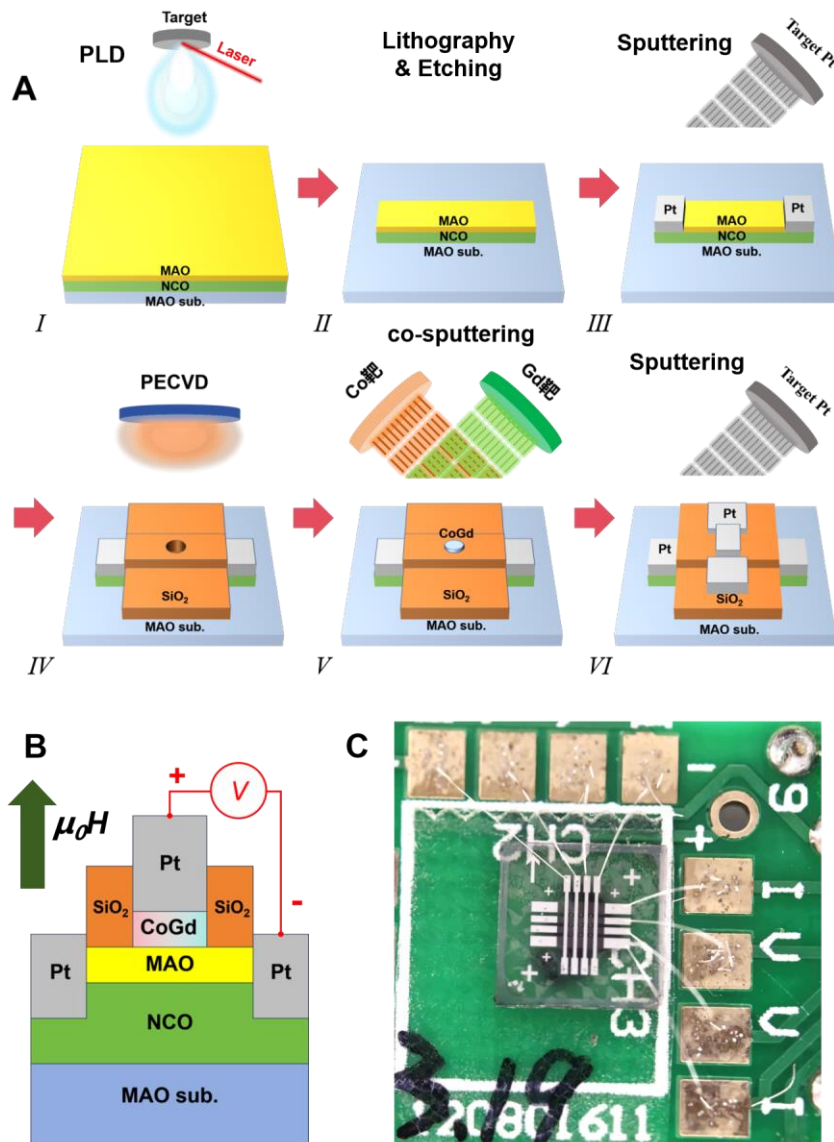
SI 9. Temperature-dependent volatile resistance multilevel states.

Table S1. Calculated magnetic moments of Gd and Co atoms, and the contribution of each state in Co₇₅Gd₂₅ alloy.

Table S2. Calculated magnetic moments of Ni_{Oh} and Co_{Td} atoms, and the contribution of each state in NCO.

Supplementary Materials

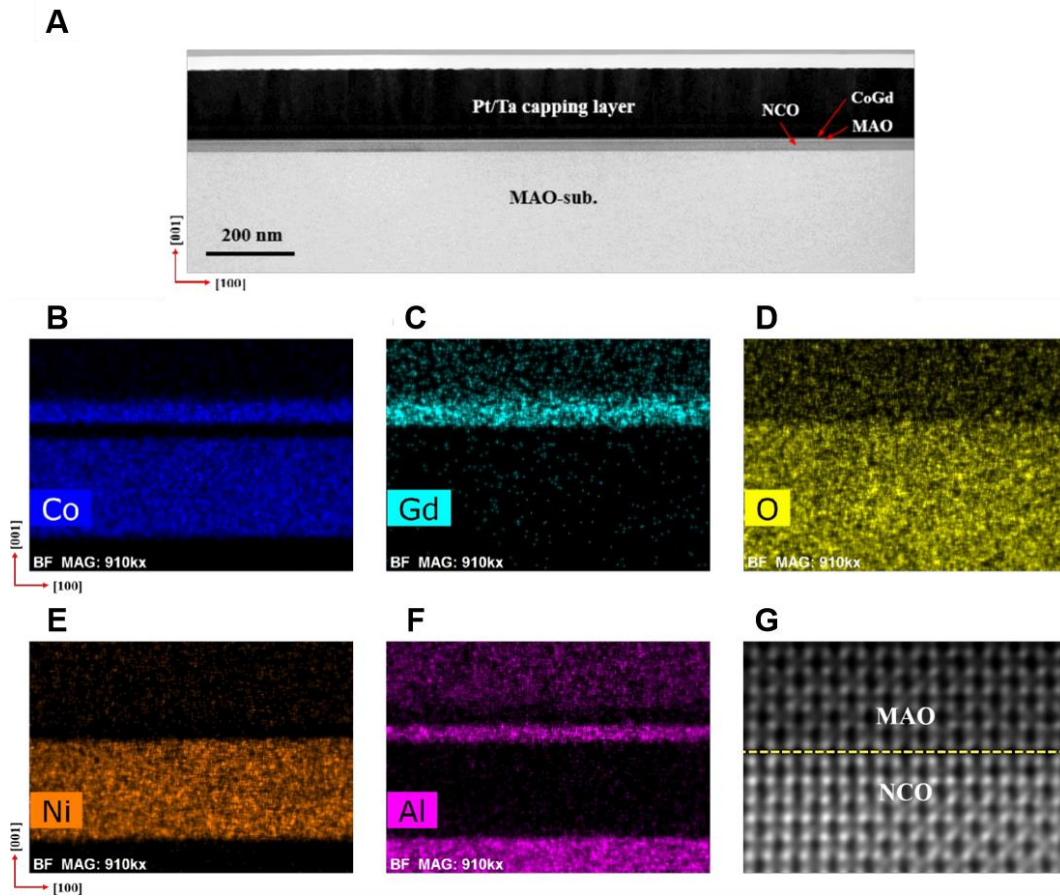
SI 1. Flow chart for fabrication of tunnel junction devices.



Supplementary Figure 1. (A) Flow Chart for Fabrication of Tunnel Junction Devices.

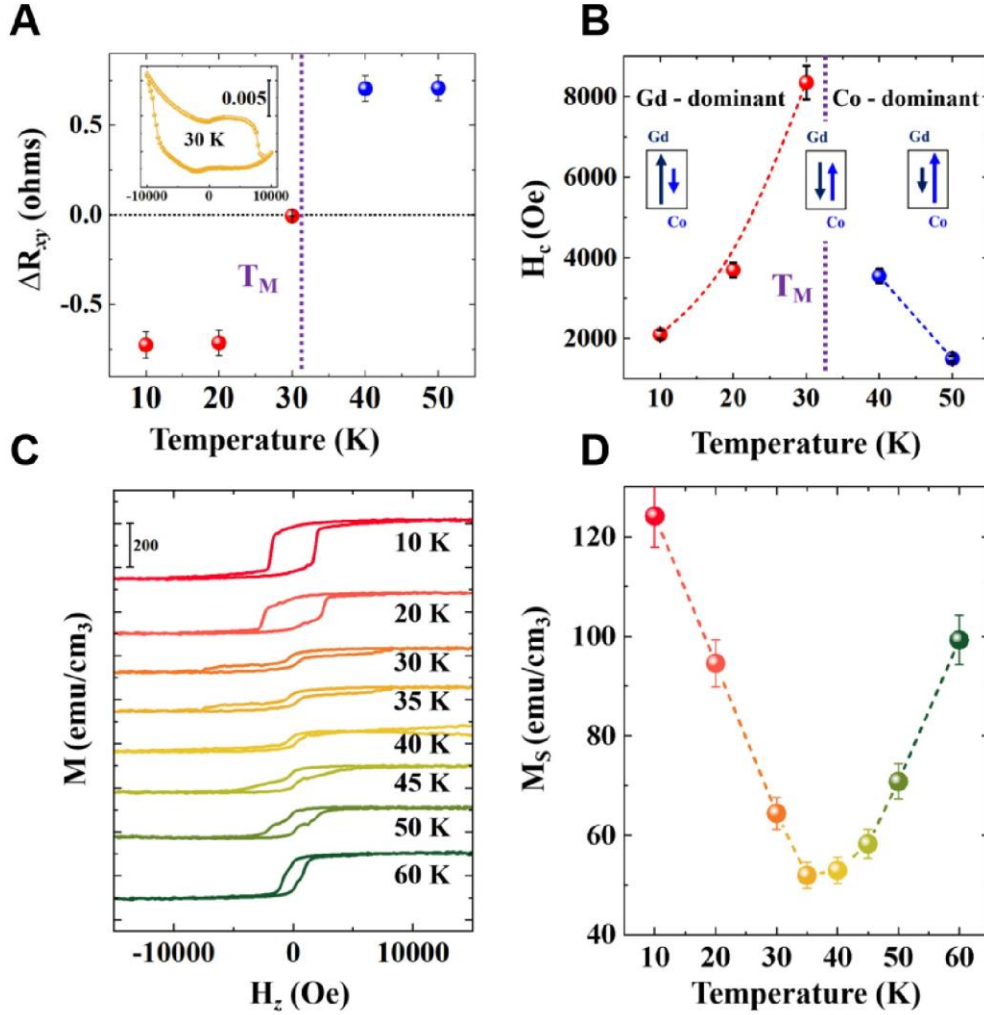
(B) Schematic diagram of the device cross-section. (C) Optical photo and measurement wiring diagram of 4×4 device array.

SI 2. TEM of the heterostructures.



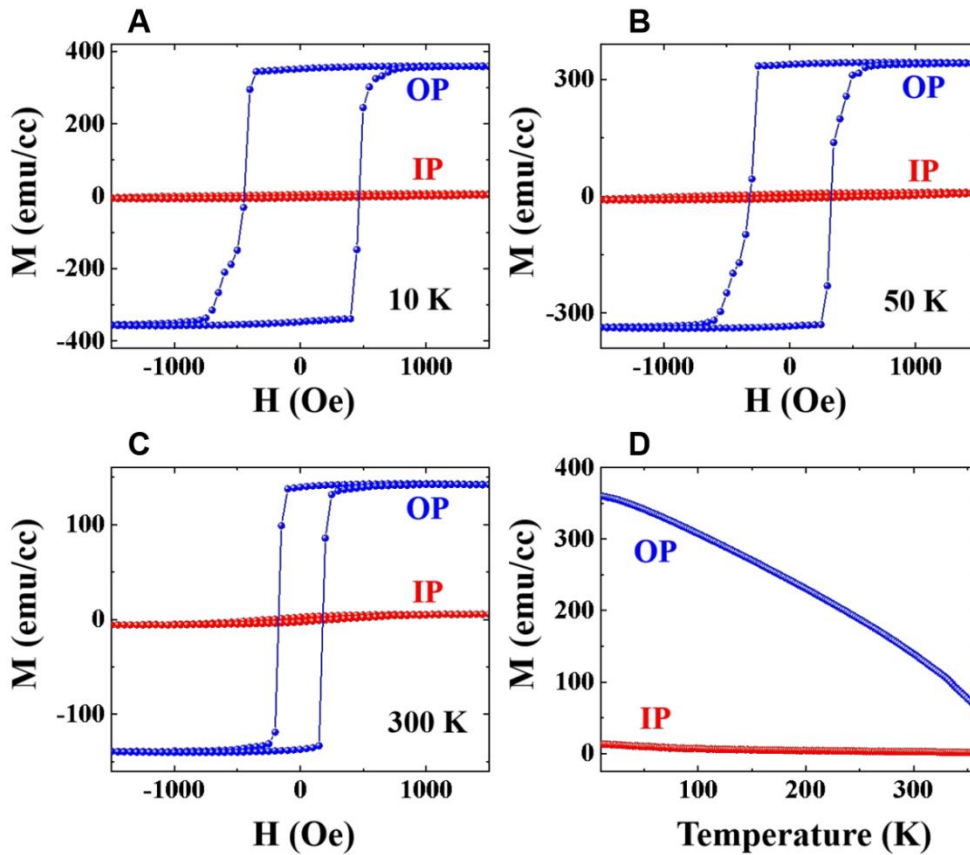
Supplementary Figure 2. (A) The low-magnification annular bright-field STEM image of the MTJ multilayers along [100] axis, where the labels indicate the different layers. The length of the scale bar is 200 nm. (B)- (F) False-color EDS maps of the Co, Gd, O, Ni, and Al elements, confirming the presence of sharp interfaces in the heterostructures. (G) HAADF-STEM image taken from interface region between NCO layer and MAO barrier.

SI 3. The temperature-dependent anomalous Hall effect (AHE) and magnetic characteristic of CoGd.



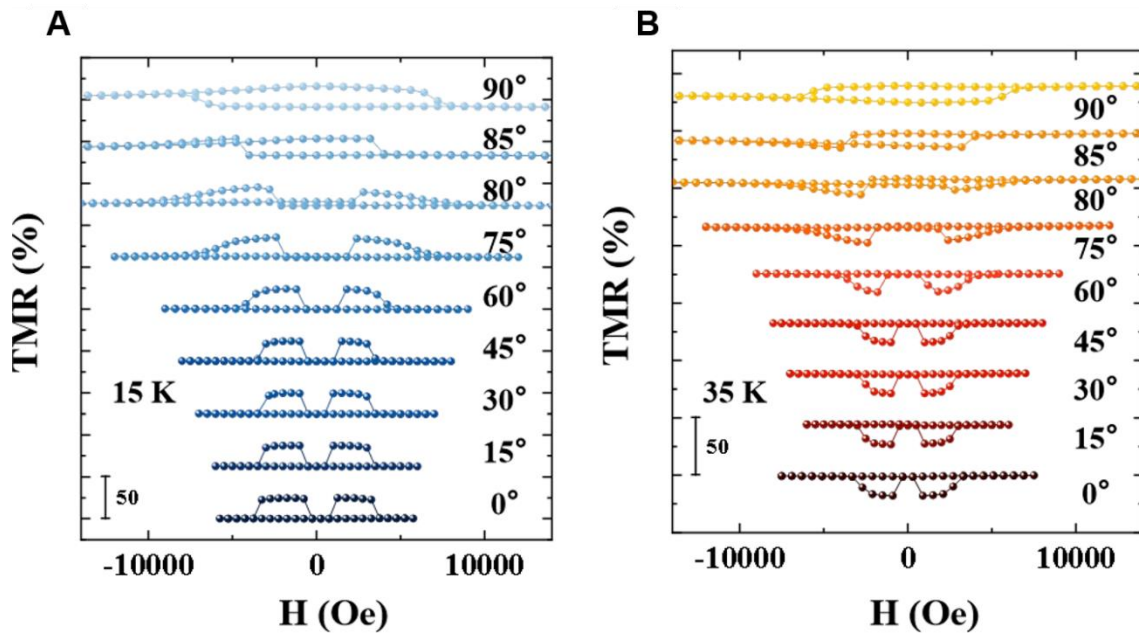
Supplementary Figure 3. (A) Temperature dependence of magnitude of Hall resistance change of Co₈₂Gd₁₈ (5 nm) /Pt (50 nm) bilayers, $\Delta R_{xy}=R_{xy}(+\mu_0 H)-R_{xy}(-\mu_0 H)$. Inset: the AHE loop at 30 K. (B) Temperature dependence of coercive field H_C . (C) Out-of-plane magnetic hysteresis loops of Co₈₂Gd₁₈ /Pt bilayers at different temperatures. (D) Temperature dependence of saturation magnetization value of Co₈₂Gd₁₈ /Pt bilayers.

SI 4. Temperature-dependent magnetization of NCO.



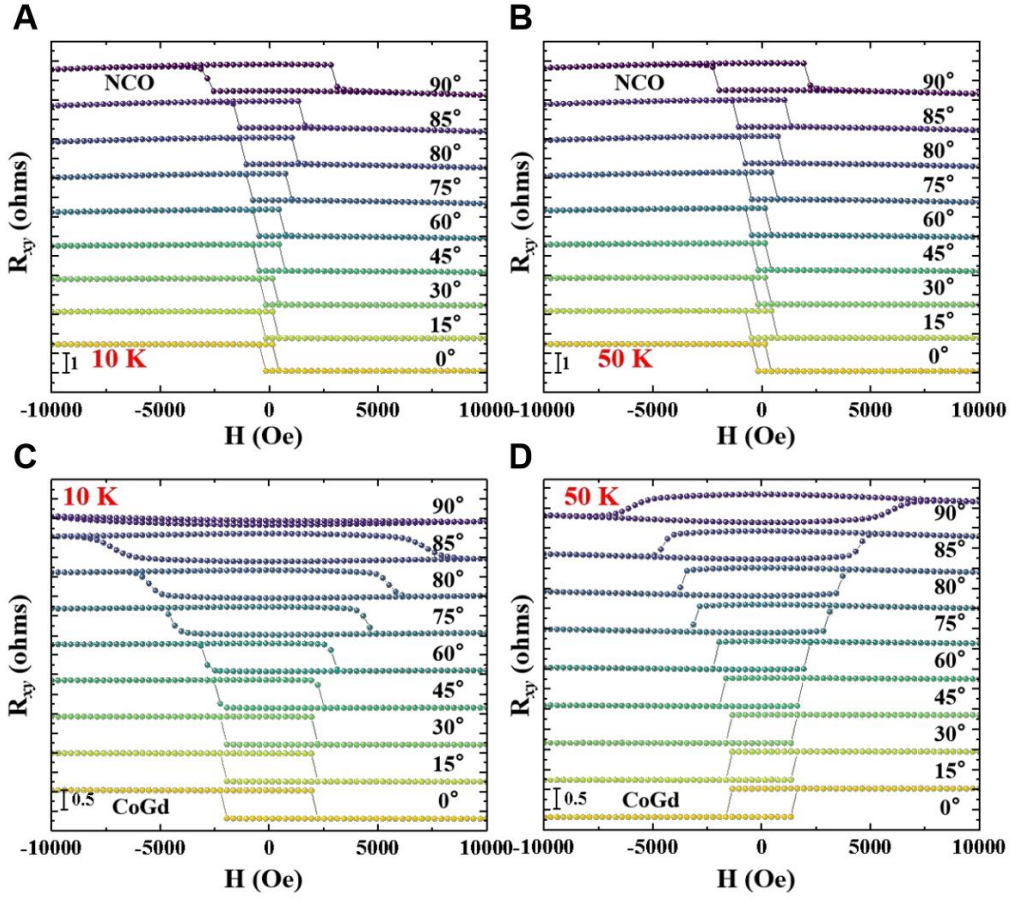
Supplementary Figure 4. Magnetic hysteresis loops with different directions at (A) 10 K, (B) 50 K, and (C) 300 K of NCO/MAO bilayers. OP and IP correspond to out-of-plane and in-plane directions, respectively. (D) Temperature dependence of the magnetizations with different directions of NCO/MAO bilayers. For all the M-T measurements, the sample was cooled from 380 to 10 K under a maintained magnetic field of 3000 Oe. Subsequently, the applied fields were decreased to zero and the magnetization was measured with increasing temperature.

SI 5. Angular dependence of the TMR.



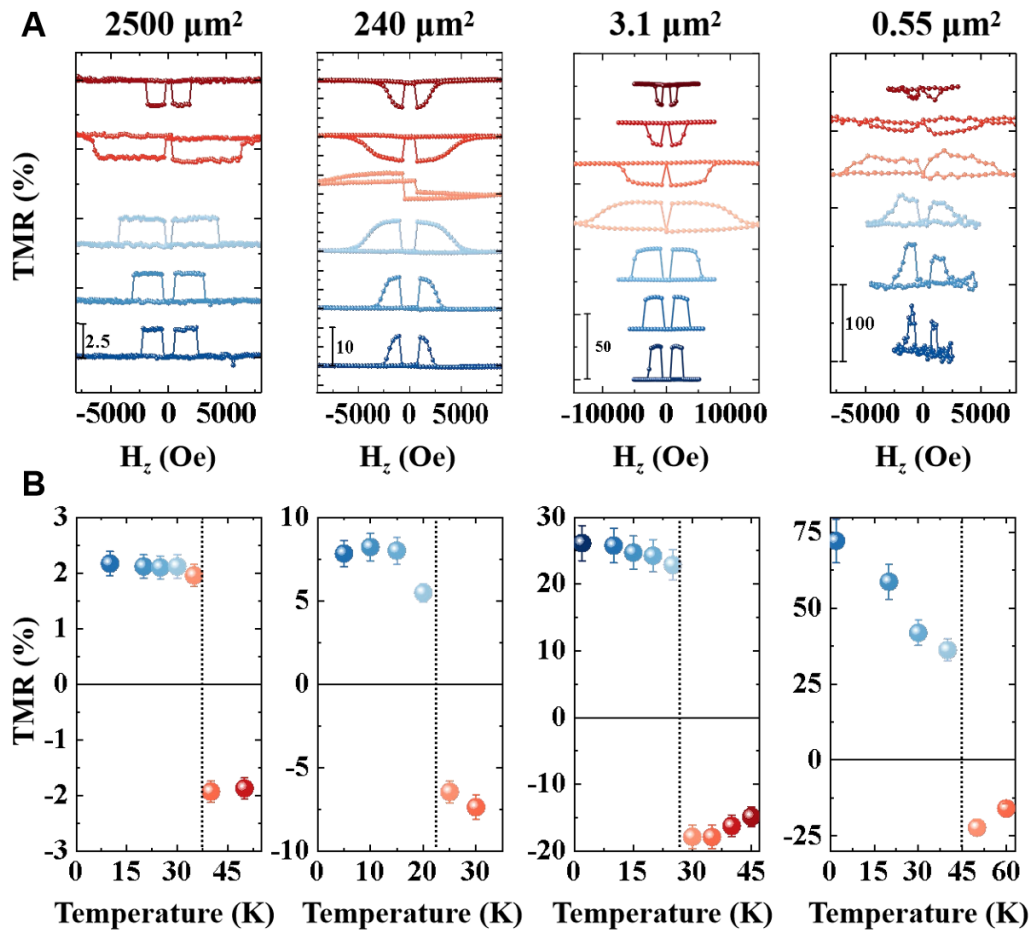
Supplementary Figure 5. The TMR loops with the magnetic field along different angles at (A) 15 K and (B) 35 K, where 0° and 90° correspond to the out-of-plane and in-plane magnetic field directions, respectively.

SI 6. Angle-dependent AHE loops.



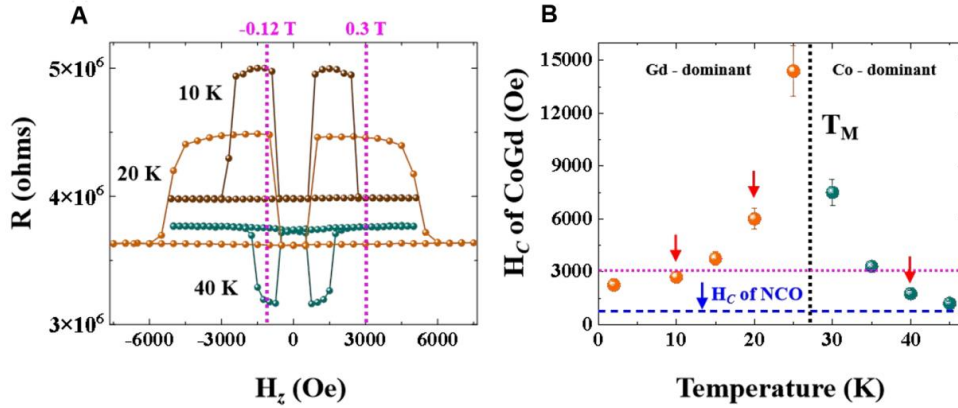
Supplementary Figure 6. The AHE loops with the magnetic field along different angles of NCO/MAO: (A) at 10 K and (B) at 50 K. The AHE loops with the magnetic field along different angles of Co₈₂Gd₁₈/Pt: (C) at 10 K (Gd - dominant) and (D) at 50 K (Co - dominant).

SI 7. The size-dependent TMR of our ferrimagnetic tunnel junctions.



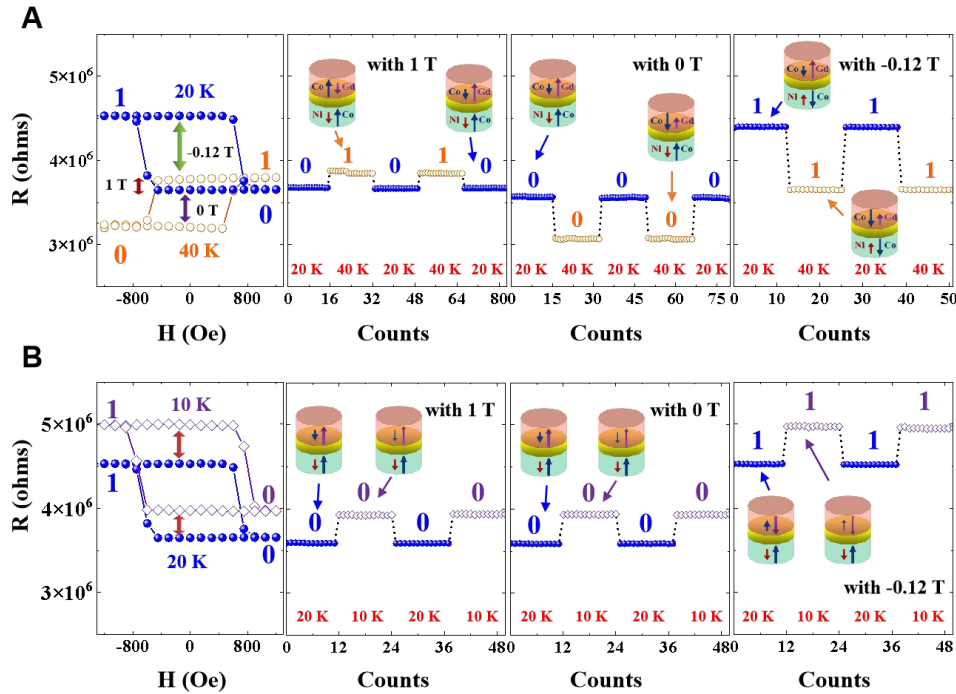
Supplementary Figure 7. (A) The TMR loops at different temperatures. (B) The temperature dependence of TMR values obtained from the MTJs with different sizes.

SI 8. The range of assisted magnetic field for thermal modulation.



Supplementary Figure 8. The assisted magnetic field marked in (A) R - H and (B) H_c - T images.

SI 9. Temperature-dependent volatile resistance multilevel states.



Supplementary Figure 9. TMR loops within a small magnetic field and temperature-dependent volatile multilevel resistance states assisted by different fixed magnetic fields (+1 T, 0 T, and -0.12 T) within (A) 20 ~ 40 K and (B) 10 ~ 20 K. “0” and “1” correspond to the low and high resistance states at the corresponding temperatures.

Supplementary Table 1. Calculated magnetic moments of Gd and Co atoms, and the contribution of each state in Co₇₅Gd₂₅ alloy

Atom	<i>s</i>	<i>p</i>	<i>d</i>	<i>f</i>	<i>M</i> (μ_B)
Gd	0.04	0.01	0.35	6.88	7.29
Co	-0.02	0.00	-1.49	0.00	-1.51

The negative values in the Co column indicates the ferrimagnetic coupling between Gd and Co atoms.

Supplementary Table 2. Calculated magnetic moments of Ni_{Oh} and Co_{Td} atoms, and the contribution of each state in NCO

Atom	<i>s</i>	<i>p</i>	<i>d</i>	<i>M</i> (μ_B)
Ni _{Oh}	0.00	0.00	-0.55	-0.55
Co _{Td}	0.03	0.08	2.30	2.41

The negative values in the Ni_{Oh} column indicates the ferrimagnetic coupling between Ni_{Oh} and Co_{Td} atoms.